Fusion Engineering and Design 85 (2010) 890–895

Contents lists available at ScienceDirect

Fusion Engineering and Design

journal homepage: www.elsevier.com/locate/fusengdes

A simple apparatus for the injection of lithium aerosol into the scrape-off layer of fusion research devices

D.K. Mansfield*, A.L. Roquemore, H. Schneider, J. Timberlake, H. Kugel, M.G. Bell, the NSTX Research Team

Princeton University, Plasma Physics Laboratory, Princeton, NJ 08543, USA

ARTICLE INFO

Article history:
Available online 24 September 2010

Keywords:
Lithium
Wall conditioning
Plasma facing components
Aerosol injection
Scrape-off layer
Spherical torus

ABSTRACT

A simple device has been developed to deposit elemental lithium onto plasma facing components in the National Spherical Torus Experiment. Deposition is accomplished by dropping lithium powder into the plasma column. Once introduced, lithium particles quickly become entrained in scrape-off layer flow as an evaporating aerosol. Particles are delivered through a small central aperture in a computer-controlled resonating piezoelectric disk on which the powder is supported. The device has been used to deposit lithium both during discharges as well as prior to plasma breakdown. Clear improvements to plasma performance have been demonstrated. The use of this apparatus provides flexibility in the amount and timing of lithium deposition and, therefore, may benefit future fusion research devices.

1. Introduction

Elemental lithium (Li) used to coat – either as a solid or liquid – plasma facing components (PFCs) has improved plasma performance in a growing number of fusion research devices [1–10]. Successful technologies have been developed to apply thin-film Li coatings onto PFCs prior to initiation of high-power discharges. Specifically, pre-deposition of Li by pellet injection into the Ohmic phase of TFTR discharges a few seconds prior to high-power neutral beam injection (NBI) as well as into several Ohmic discharges taken just before the discharge-of-interest both proved to be effective methods of improving plasma performance [1,11]. Pre-deposition of Li by evaporation before plasma breakdown has also benefitted plasma performance [2,5,6,12,13].

Other technologies designed to deposit Li into the plasma scrape-off layer (SOL) during the discharge (i.e. in real-time) have also enjoyed success. These technologies include laser-based injection of Li aerosol, injection by movable probe, use of a rotatable Li-coated limiter and use of a movable porous capillary Li limiter [14,8,10,9,15–17].

This work describes a new compact Li manipulation device which has been employed both in real-time and for pre-deposition. The device described injects an evaporating Li aerosol into the plasma SOL by simply dropping spherical Li powder in a controllable manner using a bimorph type vibrating piezoelectric disk (PZD) with a central aperture. Li injection rates as low as ~1 mg/s (4.3×10^4 spheres/s) and as high as ~120 mg/s (5.1×10^6 spheres/s) are attained reproducibly using this device. Two such devices have been used on the National Spherical Torus Experiment (NSTX) with a clear benefit to plasma performance. Li dropped and accumulated on the lower divertor of NSTX well prior to plasma initiation has also been observed to benefit plasma performance.

Controllable real-time injection of Li aerosol offers some advantages over other thin-film pre-deposition techniques. Specifically, real-time degradation of thin Li during high-power TFTR plasmas as well as the ability of continuous laser-based Li aerosol injection to compensate for that degradation have both been documented [11,14]. The efflux level attained by the device described in this work, however, is roughly six times larger than that attained by the more complicated, laser-based technique. Also, control of aerosol droplet size with this device is a feature not possible with laser-based aerosol generation. Moreover, while deposition of small amounts of Li with a movable probe has also been accomplished in real-time, that technique provided no control over Li influx during the entire duration of the discharge [8]. Such control is an important feature of the apparatus described in this work. Use of a movable porous capillary limiter can also be considered a real-time Li injection system and has been used with notable success [3,4,9,15,16]. The rate of Li deposition using that system, however, relies on sensitive control of plasma position and edge parameters—unlike the technique described in this work.

* Corresponding author at: Princeton University, Plasma Physics Laboratory, P.O. Box 451, Princeton, NJ 08543, USA. Tel.: +1 609 243 3238; fax: +1 609 243 2665.
E-mail address: dmansfield@pppl.gov (D.K. Mansfield).

0920-3796/$ – see front matter © 2010 Elsevier B.V. All rights reserved.
doi:10.1016/j.fusengdes.2010.08.033

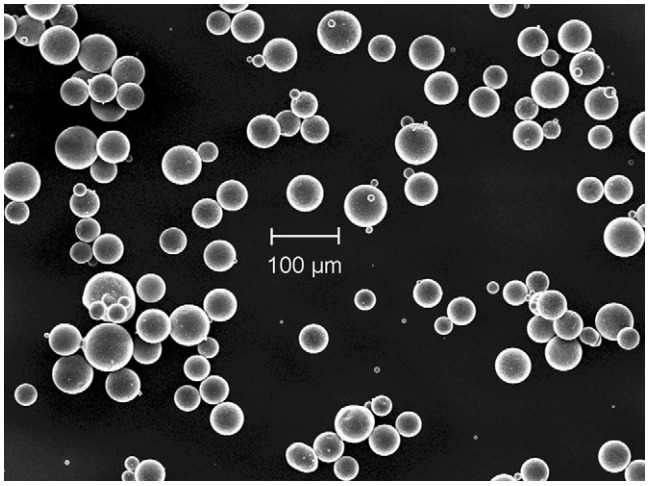

Fig. 1. The SLMP® powder used in this work.

2. The Li powder

The device viability rests on the ability of the Li powder employed to flow freely. The powder used in this work is trademarked by FMC Corporation as Stabilized Li Metallic Powder® (SLMP®) and is specifically designed to flow. Each spherical particle (44 μm average dia.) is stabilized against uncontrolled reaction with air by a ~30 nm mantle of microcrystalline Li_2CO_3. Particles are 99.9% Li and 0.1% Li_2CO_3 by composition. A scanning electron microscope image of the Li particles appears in Fig. 1.[1]

3. Eigenmodes of a disk

Manipulation of powder particles with this device depends on exploiting forced transverse vibrational modes of the PZD. When a circular disk is clamped at its periphery, discrete mechanical resonances appear at frequencies that depend on mode numbers (n, s), density (ρ), thickness (h), radius (R) and flexural rigidity (K) of the disk. Excluding solutions that are not circularly symmetric (i.e. $n = 0$ only) resonant frequencies (ω_s) are given by:

$$\omega_s = \frac{\alpha_s}{R^2}\sqrt{\frac{K}{\rho h}}, \quad s = 0, 1, 2, \ldots \tag{1}$$

where $\alpha_0 = 10.21$, $\alpha_1 = 39.78$ and $\alpha_2 = 88.90$ [18]. The resonant frequency for the (0, 2) mode used in this work is 2.25 ± 0.10 kHz and the PZD displacement at low voltage is about ± 40 μm.

4. Details of device design

The injection device is shown schematically in Fig. 2. The primary device component is a vibrating PZD (Piezo Systems Inc.—Fig. 2, I and F) with a 2.5 mm central aperture (Fig. 2, G). The diameter and thickness of the PZD are 63.5 mm and 0.41 mm, respectively. Both PZD faces are coated with 1000 Å of nickel providing electrical contact. The disk is driven transversely by applying a low ($\leq$20 V_{rms}) sinusoidal voltage across disk faces to excite a (0, 2) resonance. The containment O-ring point of contact (Fig. 2, F) is designed to coincide with the diameter (25 ± 2 mm) of the stationary resonant (0, 2) node seen in Fig. 2 lower right. The placement of this O-ring *does not* perturb the resonant PZD frequency or mode structure but *does* prevent particles on the PZD from diffusing outward when the mode is excited hence constraining those particles to move toward the aperture.

Reproducible (0, 2) excitation is accomplished by squeezing two thin annular electrodes (Fig. 2, I) against opposite PZD peripheries with two O-rings (Fig. 2, H). This method not only establishes reliable mechanical clamping, but also allows electrical contact to be made without PZD soldering. O-rings shown in Fig. 2 are *not* used to establish vacuum, but only as toroidal clamping "springs". The entire dropper assembly is enclosed in a vacuum housing attached by torus interface valve (TIV) to the NSTX vacuum vessel.

Li powder is introduced through filling holes (Fig. 2, A) and stored in a reservoir (Fig. 2, J) above the PZD. Powder is fed by gravity from the reservoir onto the PZD through an annular feed column (AFC, Fig. 2, lower left). Particle efflux is governed by a throttle gap – located at the AFC bottom and fixed in practice at 2.5 mm – consisting of a thin stainless steel skirt (Fig. 2, D) protruding down from a threaded column (Fig. 2, B) fixed in place with a locking nut (Fig. 2, C).

The reservoir capacity in Fig. 2 is ~150 cm^3 corresponding to 50 g of Li powder. Further, the weight of powder on the PZD is simply a fraction of the weight of powder in and directly above the AFC [19]. For a fixed throttle gap and frequency, therefore, particle flow rate depends only on applied voltage and is independent of the amount of powder remaining in the reservoir.

In Fig. 2, the throttle column is represented as hollow. During device development, this allowed motion of powder particles to be seen from above when the PZD was excited. These observations of particle motion and such failure phenomena as bottlenecks and agglomeration are summarized in Section 5.

A stainless steel sieve (Fig. 2, upper right) prevents particle clumps from entering the AFC where they can lodge at the throttle skirt or over the aperture and block flow. The sieve opening sizes are one quarter of the PZD aperture diameter and its 63% open area allows free powder flow. The sieve is normally located at the bottom of the reservoir at the positioned indicated in Fig. 2.

Mechanical agitation in the reservoir is provided at ~300 Hz by low voltage piezoelectric actuators (Fig. 2, upper right) which mitigate powder cavity formation and thus promote uniform particle efflux. Such agitation also minimizes long-term variations in particle flow by eliminating powder dunes that would otherwise form as the reservoir empties.

A thermocouple (TC—Fig. 2, upper right) immersed in the reservoir powder is used to guard against exothermic reactions of Li with its surroundings. The TC output is interlocked to the TIV connecting the dropper vacuum housing to NSTX. In the event of a temperature excursion (signaling, for instance, a reaction of Li with NSTX deuterium—unseen to date), the dropper control system automatically closes the TIV.

Voltage is applied to opposite PZD faces with a PC-based digital arbitrary waveform generator (AWG—Fig. 2, E) operating at output sample rates up to 2 MS/s. The AWG is appropriate for applications involving a few seconds of particle flow. Due to the finite memory of these generators, however, for applications requiring longer particle movements (say emptying the reservoir in 1 h) an analog waveform generator is sufficient.

Dropped particles pass through a 5 mW cw diode laser beam ($\lambda = 635$ nm) before entering NSTX. Light scattered orthogonal to the particle stream and that transmitted through the stream are detected by simple passive photodiodes. Scattered signals indicate *relative* particle flow while transmitted signals – in the absence of particle flow – are used to monitor laser intensity in the vibrational and magnetic NSTX environment.

[1] Similar Li powder protected by 30 nm of long-chain paraffin has been shown to be vacuum compatible and is being tested for use on NSTX. Particles of this powder are 99.4% Li and 0.6% CH_2 by composition.

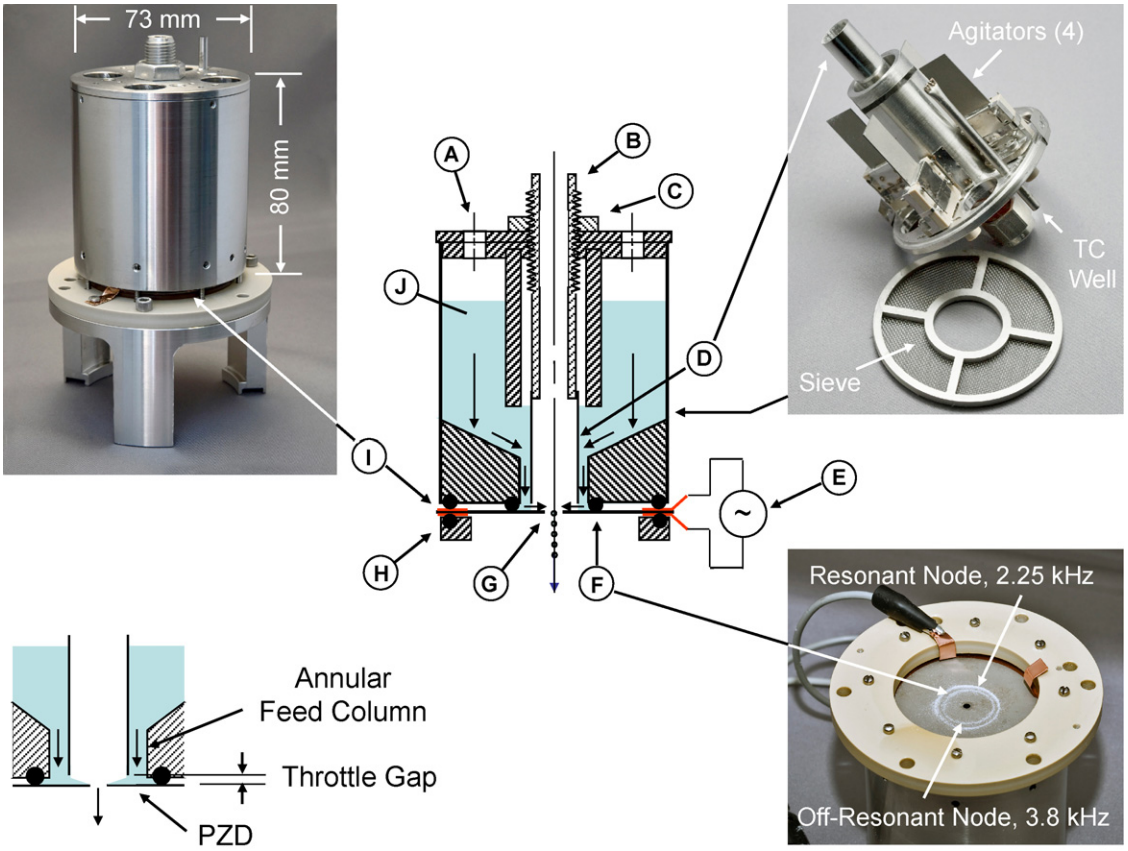

Fig. 2. The dropper/injector: details A–J are described in the text. An assembled dropper appears at upper left. An inverted throttle assembly is displayed at upper right. The agitators, thermocouple well and sieve (see text) are not represented in the schematic. The throttle gap and AFC – also explained in the text – appear at lower left. At lower right a resonant (0, 2) node can be seen by the accumulation of glass beads on an unsupported PZD (i.e. with particle containment O-ring removed from below). Also seen is a smaller non-resonant node previously driven at equal voltage but higher frequency causing lower amplitude of vibration. Redundant electrode tabs also appear.

5. Device performance

In order to preserve a limited inventory of Li powder, initial frequency and voltage scans of dropper performance as well as observations of particle movements were accomplished in air by using a substitute powder of spherical (~66 μm dia.) glass beads while measuring mass with a digital scale (Fig. 3).

Those measurements and observations serve as analogs for performance with Li powder and are justified *a posteriori* by noting the similarity of vacuum measurements performed with Li at resonance (Fig. 4) to glass-bead resonance data.

Further, the maximum glass-bead efflux attained at resonance adjusted by the ratio of Li to glass-bead powder densities yields a value that is only ~20% higher than the measured maximum Li efflux. This fact lends additional justification for the use of glass beads as a surrogate powder.

Particle motions on the PZD were observed through the hollow throttle column (Fig. 2). At low voltage particles diffuse slowly inward and simply fall off the aperture edge. At higher voltage

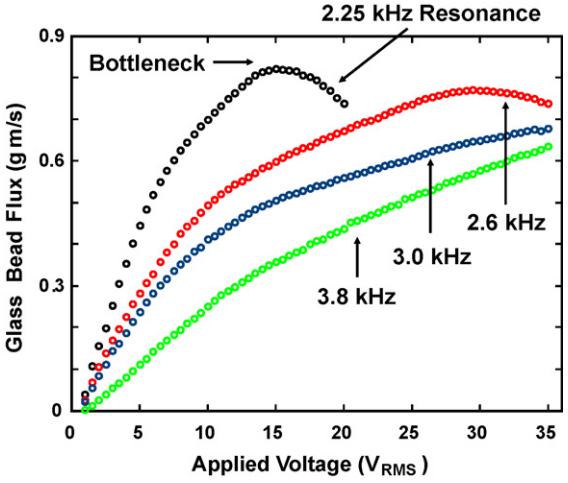

Fig. 3. Glass-bead data: each point represents the mass dropped during a 1 s constant sinusoid.

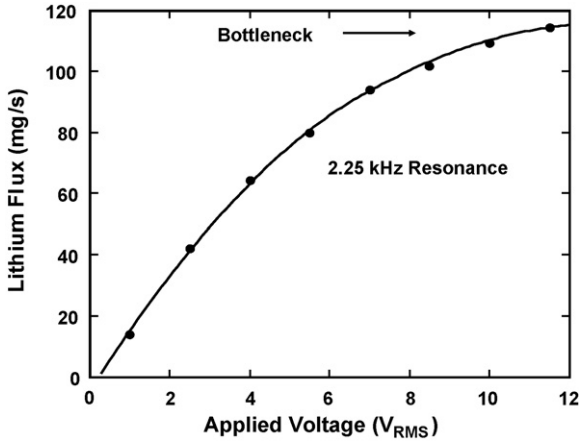

Fig. 4. Li powder data: each point represents the mass dropped during a 1 s constant resonant sinusoid.

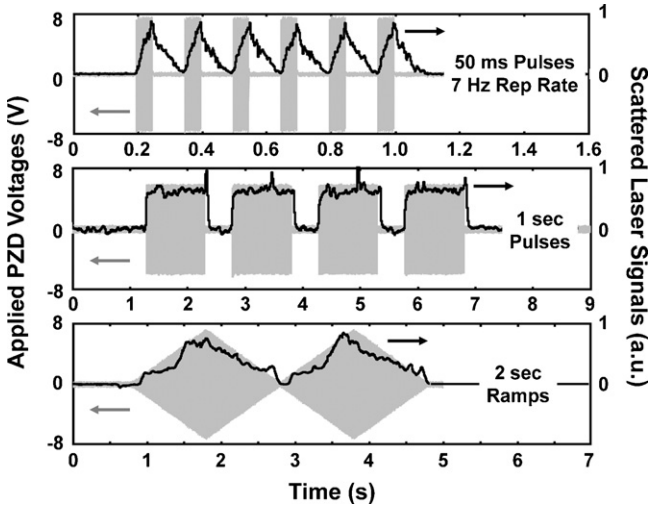

Fig. 5. Three examples of particle flow modulation using the AWG at resonance.

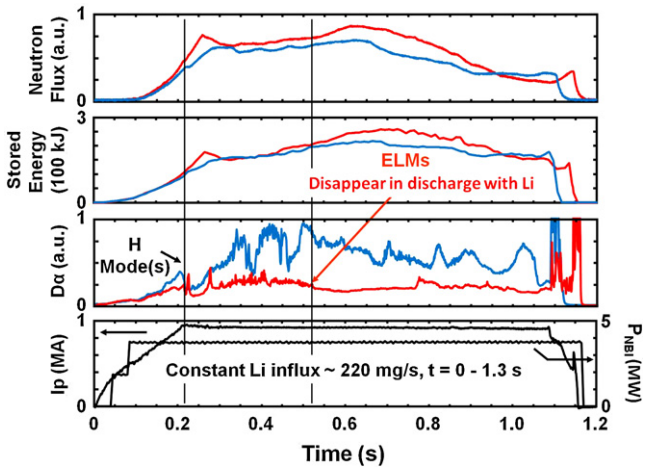

Fig. 6. Neutron rates, stored energies and Dα emissions of H-mode discharges with (red) and without (blue) Li aerosol injection. Common current and NBI powers are shown in black. (For interpretation of the references to color in this figure legend, the reader is referred to the web version of the article.)

particles jump over the edge and collide with particles jumping from the opposite side of the aperture. Eventually, however, not all particles can fit through the aperture and a bottleneck results. As voltage is raised higher, particles become tightly wedged directly over the aperture. When wedging occurs, particle efflux decreases as voltage is raised and particles become more interlocked. With some powders, such as Li, agglomeration can then take place causing permanent cessation of particle flow. Evidence of bottlenecking behavior is demonstrated in Figs. 3 and 4.

The maximum efflux of spherical particles falling *from rest* through the aperture can be estimated by considering the maximum density of spheres falling through a hole at acceleration g. The maximum density (ρ_{max}) of a powder of spheres each with density (ρ_s) is given by:

$$\rho_{max} = 0.64\rho_s, \tag{2}$$

where a packing fraction (0.64) for random close packing of identical spheres is assumed. If such a powder falls one particle diameter (D) it requires a time (t):

$$t = \sqrt{\frac{2D}{g}}, \tag{3}$$

and results in movement of mass (m) though a hole of area (A):

$$m = 0.64\rho_s DA. \tag{4}$$

Hence the maximum effective particle efflux is given by:

$$\Gamma_{max} = \frac{m}{t} = 0.45\sqrt{gD}\rho_s A. \tag{5}$$

For parameters appropriate to the glass beads (or Li powder) used in this work, the maximum estimated effluxes given by Eq. (5) are:

$$\Gamma_{max} = 150\,\text{mg/s}\,(24\,\text{mg/s}) \tag{6}$$

Because the measured maximum effluxes in Fig. 3 (4) – 850 mg/s (113 mg/s) – are larger than the estimated maxima it suggests that, for voltages lower than required for a bottleneck, particles are *driven* through the aperture and not simply falling from rest. Therefore, Li powder efflux data were taken only up to 12 V_{rms} to avoid forced permanent agglomeration.

Dropper laser signals taken in the laboratory appear in Fig. 5 and demonstrate a range of particle efflux profiles achievable using the AWG.

6. Aerosol injection and results on NSTX

Li aerosol injection has clearly improved NSTX performance. Fig. 6 displays plasma parameters for 2009 discharges with and without Li injection but with identical current, toroidal field, NBI input powers and H-mode transition times.

The Li-enhanced discharge (shown in red) was injected with a constant, equal influx of Li from two droppers (~220 mg/s total). Several reproducible features seen in Fig. 6 are consistent with previous experience using other Li delivery techniques. Included among these are the suppression (after $t \sim 500$ ms) of edge localized modes (ELMs) with concomitant increases in stored energy and beam-target neutrons due to higher electron and ion temperatures [12,13].

In Fig. 7 use of two droppers 180° apart is demonstrated in a sequence of video images from an NSTX discharge (Fig. 6 shown in red). As seen in the images, solid Li particles in the SOL are heated and ablated by electron impact. Particles quickly liquefy and develop an incandescent neutral ablation cloud, appearing yellow [17,20]. This process continues until complete droplet evaporation occurs. Lithium ions (Li^{1+}) can be identified in the images by their strong 5485 Å green line emission.

On the right of each video frame Li particles fall straight into the SOL and Li^{1+} ions drift along field lines as Li evaporates and ionizes. The left side of each frame shows effects of a 45° "splash plate" terminating a 12 mm ID drift tube leading from the dropper. This plate disperses falling particles horizontally inward.

In the first frame Li droplets fall straight down on the right. At the time of the image (t = 23 ms) the plasma has not expanded to its full volume; hence droplets fall vertically through SOL plasma (i.e. the separatrix has not reached the point directly below the dropper drift tube). In this frame NBI injection had not begun; hence, no SOL flow exists and droplets are not swept into that flow. Droplets can be seen on the left that have been dispersed off of the 45° plate and are thus initially injected approximately horizontally into the SOL.

Later (t = 79 ms), as the plasma column continues to expand, NBI begins and Li droplets on the right are swept into the resulting SOL flow and behind the center stack. The direction of beam injection is into the plane of the page and to the right of the center stack. Also seen in this frame are Li droplets that had been intentionally predeposited using the droppers onto the NSTX lower divertor well before the beginning of the discharge. In this frame ~250 mg of this Li is shown uniformly distributed around the base of the center

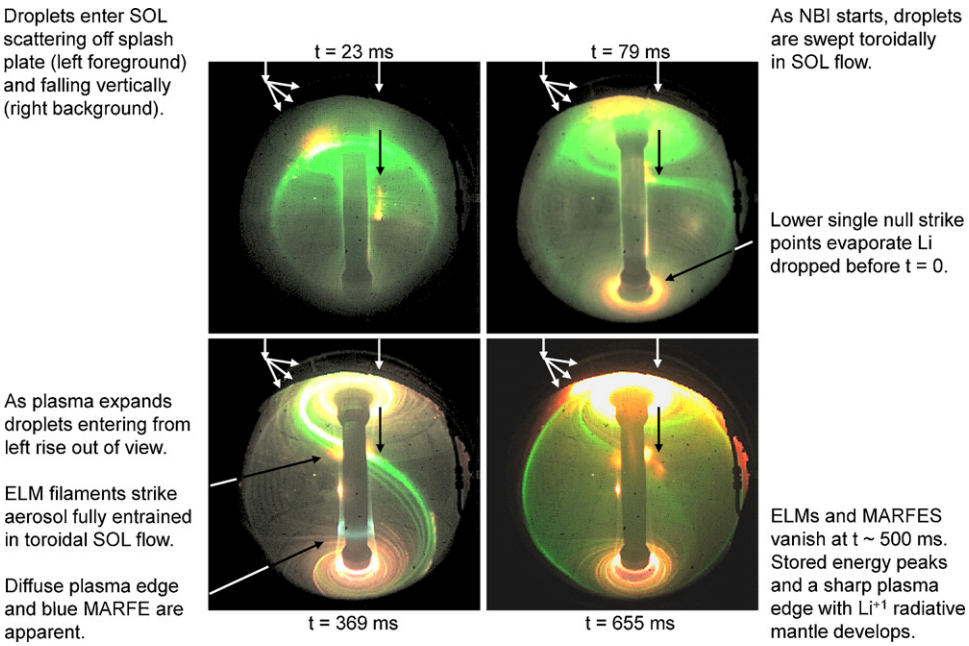

Fig. 7. Video images of NSTX discharge 135063 showing effects of Li aerosol injection—also represented in Fig. 6 in red. The particular plasma shown in these video images received a remarkably large amount of Li (~220 mg/s) although no optimization is claimed. Similar improvements to plasma performance were observed in contemporaneous discharges using significantly lower rates of Li injection.

stack just as the plasma column becomes diverted (i.e. just before the newly formed strike points sweep inboard onto the droplets). The resulting rapid evaporation and ionization of these droplets caused saturation of the video camera with 5485 Å radiation for the next ~150 ms but caused no apparent deleterious effects on plasma performance. Rather, in a limited trial, this pre-positioning technique produced benefits similar to those realized by pre-deposition of evaporated Li routinely carried out between NSTX discharges.

After the plasma enters the H-mode (at ~215 ms) both MARFEs and ELMs develop as seen in the next frame (t = 369 ms). By this stage in the discharge, Li particles that originally simply fell vertically in the SOL (first frame—on the right) are seen horizontally entrained in SOL flow as a Li aerosol evaporating behind the center stack. The effects of ELM filaments impinging on this aerosol are clearly seen in this frame. Droplets injected at upper left are not visible because expansion of the plasma column has, by this stage of the discharge, forced those particles upward and out of the camera field of view. The remnant of a high-field-side deuterium gas puff can also be seen on the left side of the center stack.

In the final frame (t = 655 ms), as Li accumulates on PFCs, the simultaneous disappearance of both MARFEs and ELMs (at ~500 ms) results in improved plasma confinement (see Fig. 6). The plasma stored energy, neutron production rate, electron and ion temperatures all reach a peak. Simultaneously, the plasma edge becomes quiescent and adopts a distinct Li^{1+} radiating mantle. In addition, by this stage of the discharge, the increased temperature of the SOL is evidenced by the re-appearance of ablating particles that had previously been out of the camera field of view in the upper left. In fact ablation is so strong that camera saturation (appearing white) is clearly seen in the entire upper part of the SOL.

NSTX discharges appear to be remarkably tolerant of large influxes of Li aerosol introduced into the SOL by this dropping/injection technique. As an example, the Li atomic influx in shot 135063 (Figs. 6 and 7) from dropping in real-time alone exceeds – by at least a factor of five – the deuterium influx from gas puffing (3.6×10^{21}/s D) and NBI (3×10^{20}/s D) combined (2.0×10^{22}/s Li vs. 3.9×10^{21}/s D).

7. Summary and discussion

A simple device has been developed to exploit the recent commercial availability of Li powder. The device has been used to inject an evaporating Li aerosol into the NSTX SOL by simply dropping fine Li powder in a controlled manner either during NBI-heated discharges or before plasma breakdown.

Improvements to NSTX plasma performance (Fig. 6) realized with aerosol injection – including ELM suppression – are similar to those possible with other Li coating techniques.

Because NSTX plasmas are relatively short-lived (1–2 s), it seems that the advantages of continuous real-time aerosol injection might be more fully exploited in future long-pulse fusion devices which will likely need continuous resupply in order to benefit from Li conditioning.

Although the dropping system enhanced NSTX performance, changes to the injection geometry would likely lead to additional improvement. As seen in Fig. 7, when Li particles are dropped/injected from above the plasma mid-plane, NBI-driven SOL flow directs both liquid aerosol particles and Li ions predominantly upward—away from the divertor strike points of standard lower single null plasmas. Because the lower strike points are *exactly* where deposition of Li is expected to be most effective, the existing injection geometry is clearly not optimal. This difficulty prompted the use of the apparatus to simply drop Li powder onto the lower divertor before plasma breakdown—as shown in Fig. 7 at t = 79 ms.

The location of the SOL injection point could be optimized by employing a rotating dielectric paddlewheel to redirect and disperse falling Li particles. Such a simple additional technology would make aerosol injection possible in all directions. Injecting aerosol horizontally at the plasma mid-plane or supplying lower single null strike points from below are two such possibilities.

Acknowledgements

The authors would like to thank Mike Vocaturo of Princeton, Jim Irby of MIT, Zhehui Wang and Glen Wurden of LANL, Marina Yakovl-

eva and Yuan Gao of FMC Corp. as well as Richard Kensley and Rob Carter of Piezo Systems Inc. for useful discussions and ideas.

This work was supported by U.S. Department of Energy Contract DE-AC02-09CH11466.

References

[1] D.K. Mansfield, J.D. Strachan, M.G. Bell, S.D. Scott, R. Budny, E.S. Marmar, et al., Phys. Plasmas 2 (1995) 4252–4256.
[2] H. Sugai, Toyoda, K. Nakamura, K. Furuta, M. Ohori, K. Toi, et al., J. Nucl. Mater. 220–222 (1995) 254–258.
[3] F.L. Tabarés, M.A. Ochando, F. Medina, D. Tafalla, J.A. Ferreira, E. Ascasibar, et al., Plasma Phys. Control. Fusion 50 (2008) 124051.
[4] G. Mazzitelli, Proc. 22nd Int. Conf. on Fusion Energy, Geneva, October, 2008, Vienna, IAEA file EX-P4-6.
[5] H.W. Kugel, M.G. Bell, J.W. Ahn, J.P. Allain, R. Bell, J. Boedo, et al., Phys. Plasmas 15 (2008) 056118.
[6] H.W. Kugel, D. Mansfield, R. Maingi, M.G. Bell, R.E. Bell, J.P. Allain, et al., J. Nucl. Mater. 390–391 (2009) 1000–1004.
[7] R. Majeski, R. Doerner, T. Gray, R. Kaita, R. Maingi, D.K. Mansfield, et al., Phys. Rev. Lett. 97 (2006) 075002-1–075002-4.
[8] R. Terreault, H.Y. Guo, D. Keroack, R.W. Paynter, W.W. Zuzak, G. Abel, et al., J. Nucl. Mater. 220–222 (1995) 1130–1134.
[9] V.A. Evtikhin, I.E. Lyublinski, A.V. Vertov, S.V. Mirnov, V.B. Lazarev, N.P. Petrova, et al., Plasma Phys. Control. Fusion 44 (2002) 955–977.
[10] Y. Hirooka, H. Zushi, R. Bhattacharyay, M. Sakamoto, H. Idei, T. Yoshinaga, et al., J. Nucl. Mater. 390–391 (2009) 502–506.
[11] D.K. Mansfield, K.W. Hill, J.D. Strachan, M.G. Bell, S.D. Scott, R. Budny, et al., Phys. Plasmas 3 (1996) 1892–1897.
[12] D.K. Mansfield, H.W. Kugel, R. Maingi, M.G. Bell, R. Kaita, J. Kallman, et al., J. Nucl. Mater. 390–391 (2009) 764–767.
[13] M.G. Bell, H.W. Kugel, R. Kaita, L.E. Zakharov, H. Schneider, B.P. LeBlanc, et al., Plasma Phys. Control. Fusion 51 (2009) 124054–124065.
[14] D.K. Mansfield, D.W. Johnson, B. Grek, H.W. Kugel, M.G. Bell, R.E. Bell, et al., Nucl. Fusion 41 (2001) 1823–1834.
[15] S.V. Mirnov, E.A. Azizov, V.A. Evtikhin, V.B. Lazarev, I.E. Lyublinski, A.V. Vertov, et al., Plasma Phys. Control. Fusion 48 (2006) 182.
[16] S.V. Mirnov, V.B. Lazarev, S.M. Sotnikov, V.A. Evtikhin, I.E. Lyublinski, A.V. Vertov, Fusion Eng. Des. 65 (2003) 455.
[17] B.V. Kuteev, V.Yu. Sergeev, S.V. Krylov, V.G. Skokov, V.M. Timokhin, Nucl. Fusion 50 (2010) 075001.
[18] W. Weaver, S.P. Timoshenko, D.H. Young, Vibration Problems in Engineering, John Wiley & Sons, New York, 1990, pp. 504–505.
[19] H.M. Jaeger, S.R. Nagel, Science 255 (1992) 1524.
[20] A. Tanaka, Yu. Pigarov, R.D. Smirnov, S.I. Krasheninnikov, N. Ohno, Y. Uesugi, Phys. Plasmas 14 (2007) 052504.